THE GADOLINIUM-LEAD PHASE SYSTEM

by

John T. Demel

A Thesis Submitted to the

Graduate Faculty in Partial Fulfillment of

The Requirements for the Degree of

MASTER OF SCIENCE

Major Subject: Metallurgy

Iowa State University
of Science and Technology
Ames, Iowa

1968

TABLE OF CONTENTS

INTRODUCTION

An investigation of the gadolinium-lead phase diagram can be justified for two reasons. The first is a practical reason. Gadolinium has a neutron absorption cross-section (46, 000 barns) that is more than one thousand times that of lead (1, p. 233). Thus, any amount of gadolinium alloyed with lead would mean a more efficient reactor shielding for any given thickness. This alloy shielding will be practical if the reactor applications justify the cost of gadolinium or if gadolinium can be produced more economically. The second reason involves the theoretical aspects of alloying. Alloy theories and alloy rules have been proposed and each new phase diagram either supports or rejects these criteria.

The experimental procedures will be presented first and then the results obtained by these procedures. These results will be discussed with respect to current alloy theories, that is, how well could this particular binary phase diagram have been predicted?

EXPERIMENTAL PROCEDURE

Materials

The major impurities in the gadolinium and lead used in this investigation are given in Appendix I. The gadolinium was prepared at this laboratory by the calcium reduction of the fluoride followed by distillation of the gadolinium. Four different gadolinium samples were used and they are labeled 1, 2, 3 and 4 in Appendix I. The lead was supplied by Comnico Products, Inc.

Alloy Preparation

The alloys were prepared by melting weighed amounts of gadolinium and lead in sealed tantalum crucibles. Homogenization was obtained by holding the constituents in the liquid state for 30 minutes, cooling, inverting the crucibles, remelting and repeating the process at least twice. The specimens for x-ray powder work were prepared in a dry-argon atmosphere because most of the alloys were found to be reactive in air.

Thermal Analysis

Differential thermal analysis (DTA) was used to determine the liquidus curves and reaction horizontals of the system. Both Pt vs. Pt + 13 w/o Rh and W + 5% Re vs. W + 26 w/o Re thermocouples were used to measure the temperature. The Pt vs. Pt + 13 w/o Rh thermocouples were used for temperatures to 1400°C while W + 5 w/o Re vs. W + 26 w/o Re thermocouples were used for temperatures over 1400°C.

The Pt vs. Pt + 13 w/o Rh thermocouples were calibrated using lead (327°C), silver (961°C), copper (1083°C) and gadolinium (1313°C) standards. These thermocouples gave temperatures within ±2°C of each melting points. The W + 5 a/o Re vs. W + 26 a/o Re thermocouples were calibrated using transformations in samples which were measured previously using the platinum alloy thermocouples and for temperatures over 1400°C a sample of LaF_3 was used as a standard. The tungsten-rhenium alloy thermocouples produced temperatures within ±5°C of the transformations and the melting point (1493°C) of LaF_3(2). Temperatures for eutectic and peritectic horizontals were reproducible to ±2°C below 1140°C and to ±7°C above 1140°C. Liquidus temperatures were reproducible to ±10°C. Both types of thermocouples were shielded with high purity alumina insulators supplied by Norton and specified to be 99.94 a/o pure alumina. An X-Y recorder was used to record the plot of temperature vs. differential temperature and the arrests were measured using a precision potentiometer.

Liquidus temperatures were obtained from cooling arrest data while both heating and cooling arrest data were used to establish the reaction horizontals. Heat treatments of alloys between 37.5 a/o and 70 a/o Pb during thermal analyses were necessary to approach equilibrium conditions. On cooling, samples were held at temperatures just below the various peritectic horizontals for a minimum of two hours before thermal analysis was continued.

The entire range of composition was investigated with a minimum amount of materials by adding appropriate amounts of lead or gadolinium to master alloys. Metallographic examination of these

DTA samples showed no extensive reaction of the alloys with the tantalum crucibles.

X-Ray and Metallographic Methods

Slice specimens for metallography and powder specimens for x-ray diffraction were prepared from two gram samples sealed in tantalum capsules and melted. For low temperature heat treatments (< 1000°C) the tantalum capsules were sealed in argon filled quartz tubes. For high temperature heat treatments the tantalum capsules were heated by using induction or resistance heating in vacuums of 10^{-5} torr. The samples sealed in quartz were quenched by breaking in water immediately upon removal from the heat-treating furnaces, and the second group of alloys were rapidly cooled by turning off the power.

All the metallographic specimens were mechanically polished. The gadolinium-rich samples were etched with concentrated nitric acid, while those samples from 14 a/o to 78 a/o Pb were air-etched. Samples from 40 a/o to 70 a/o Pb, being very reactive with the air, were photographed either through plastic medical slides and a very thin layer of kerosene or through a sight glass fused in the bottom of a beaker containing chilled absolute alcohol.

Specimens for x-ray diffraction were prepared by crushing or filing the various alloys in an inert gas atmosphere. The powders from alloys containing less than 20 a/o Pb or more than 45 a/o Pb were heat treated at ~ 500°C to remove strains by sealing the powders in tantalum tubes and heating the samples inductively in a vacuum. Those samples in the 20 a/o to 45 a/o Pb range were used without annealing due

to their brittle nature. Powder patterns were then taken by using copper and iron radiation. A computer program written by Jeitschko and Parthé (3) was used to generate the crystallographic data for the possible intermetallic compound structures of the various compounds in this system. The observed $\sin^2\theta$ and intensity data for the reflections were compared to the calculated values for an assumed structure and when good agreement was reached the structure for the compound was considered solved. The extrapolated lattice parameters were determined by using the Vogel-Kempter (4) extrapolation program for the Nelson-Riley function.

RESULTS

The results of the investigation of the Gd-Pb alloy system are summarized by Fig. 1. This diagram was constructed from differential thermal analysis data. X-ray and metallographic results confirmed the thermal analysis data and helped locate the stoichiometries of the six compounds found in this alloy system.

Terminal Reactions

The melting point of lead was raised 1°C by the addition of gadolinium. This is interpreted to be peritectic reaction and was detected by using a sample of pure lead as the standard in DTA when a sample of 97.44 a/o Pb was run.

The addition of small amounts of lead to gadolinium lowered the alpha to beta transformation temperature of 1258°C (5) to 1212°C by an inverse peritectic reaction. This may not be the true temperature for this reaction because tantalum lowers the transformation temperature of gadolinium to 1236 (5), and it is quite likely that the gadolinium-rich alloys used in this study are saturated with tantalum since tantalum thermal analysis crucibles were used.

The melting point of gadolinium is lowered by lead additions yielding a eutectic reaction at 14.5 a/o Pb and 1120°C. The eutectic composition is based upon the extrapolation of the liquidus data to the eutectic temperature, and it was confirmed by a photomicrograph of a 15.5 a/o Pb alloy which shows a small amount of the Gd_5Pb_3 compound in a eutectic matrix (see Fig. 2).

Figure 1. The gadolinium-lead binary phase diagram.

Differential thermal analysis data.

X - liquidus points - cooling arrests.

○ - horizontal points - cooling and heating arrests.

△ - horizontal points - heating arrests.

▽ - horizontal points - cooling arrests.

● - arrests due to transformations in Gd.

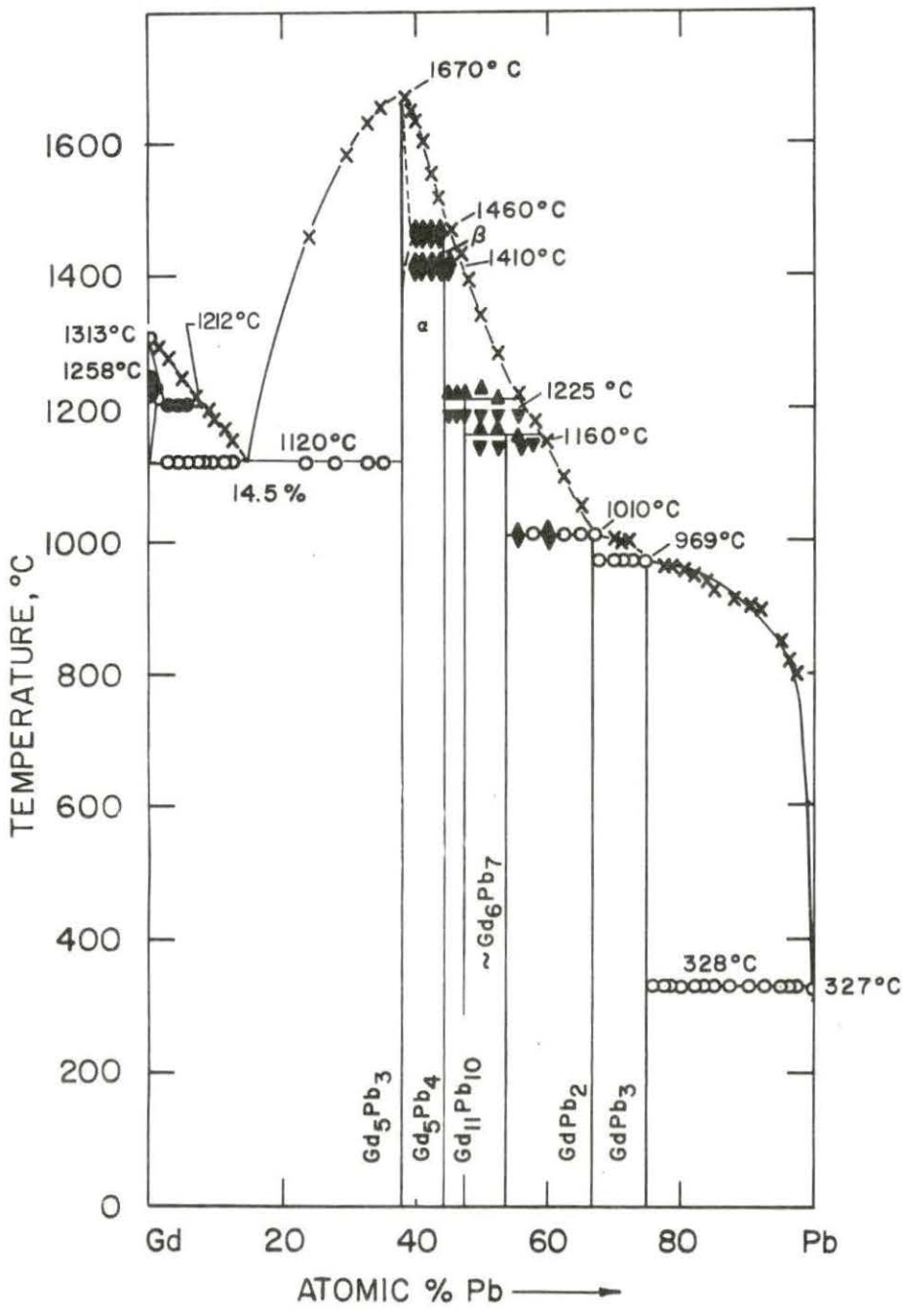

Figure 1. The gadolinium-lead binary phase diagram.

Terminal Solid Solubilities

The limits of solid solubility of lead in the two phases of gadolinium were 0.5 a/o Pb at 1080°C (α, hcp phase) and ~ 2.0 a/o Pb at 1212°C (β, bcc phase). The solubility in the hcp phase was estimated from photomicrographs of alloys of 0.08, 0.8, 1.5 a/o Pb, which were heat treated at and quenched from 1080°C (see Figs. 3, 4, 5). The first shows no precipitate while an increasing amount of precipitate is seen in the 0.8 to 1.5 a/o Pb alloys. The solubility in the bcc phase was estimated from thermal analysis data.

X-ray powder patterns of 98.83, 99.17 and 99.71 a/o Pb alloys showed the same structure and parameter as pure lead. This indicates that there is very little solubility of gadolinium in lead.

Intermetallic Compounds

Six intermetallic compounds were identified in the Gd-Pb system and have the following formulae: Gd_5Pb_3 (37.5 a/o Pb), Gd_5Pb_4 (44.4 a/o Pb), $Gd_{11}Pb_{10}$ (47.5 a/o Pb), ~ Gd_6Pb_7 (~ 54 a/o Pb), $GdPb_2$ (66.6 a/o Pb) and $GdPb_3$ (75 a/o Pb). X-ray powder diffraction methods were used to establish the crystal structure of three of the six compounds. Evidence for the existence, structure and melting characteristics is summarized below.

Metallographic evidence for the compounds is presented in Figs. 2, 6-17. For each compound there is a photomicrograph of an alloy on either side of the compound in addition to the photomicrograph of an alloy on or very near the composition of the compound. Microscopic examination of alloys from 40 to 43 a/o Pb which were heat treated and

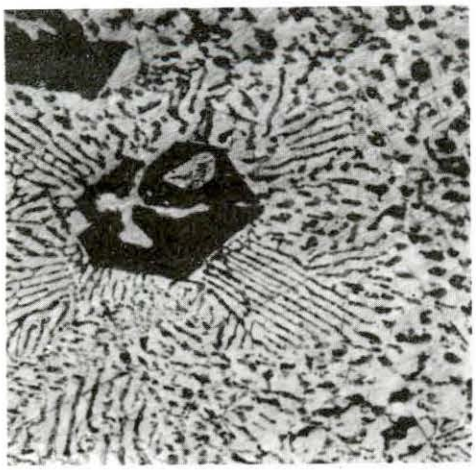

Figure 2. 15.46 a/o Pb, furnace cooled, air etched, Gd-Gd_5Pb_3 eutectic; light area --- Gd, X200.

Figure 3. 0.08 a/o Pb, quenched from 1080°C, etched with concentrated HNO_3, X1000.

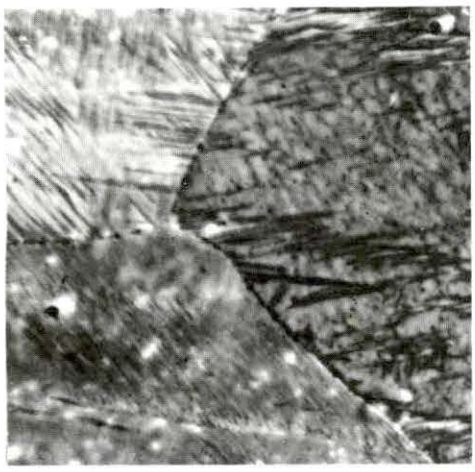

Figure 4. 0.82 a/o Pb, quenched from 1080°C, etched with concentrated HNO_3, X1000.

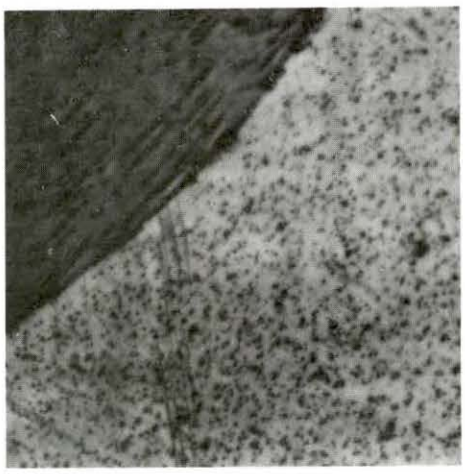

Figure 5. 1.37 a/o Pb, quenched from 1080°C, etched with concentrated HNO_3, X1000.

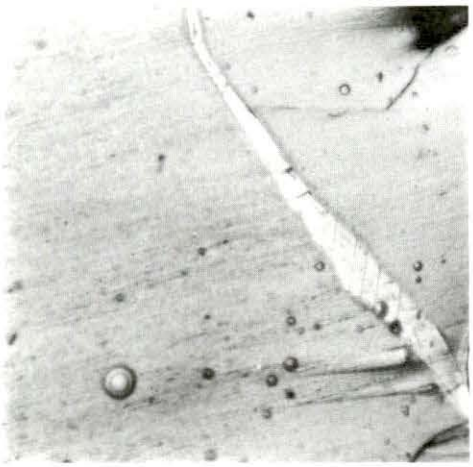

Figure 6. 37.45 a/o Pb, furnace cooled, air etched, nearly pure Gd_5Pb_3, light area --- Gd-Gd_5Pb_3 eutectic, X500.

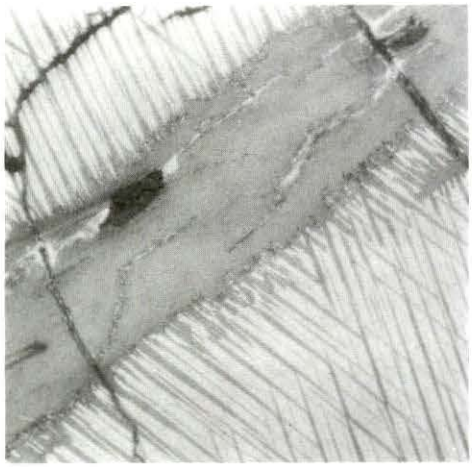

Figure 7. 41.52 a/o Pb, furnace cooled, air etched, light area --- Gd_5Pb_3, dark area Gd_5Pb_4, X250.

Figure 8. 44.34 a/o Pb, furnace quenched from 1430°C, air etched, dark area --- Gd_5Pb_4, light area --- Gd_5Pb_3, X200.

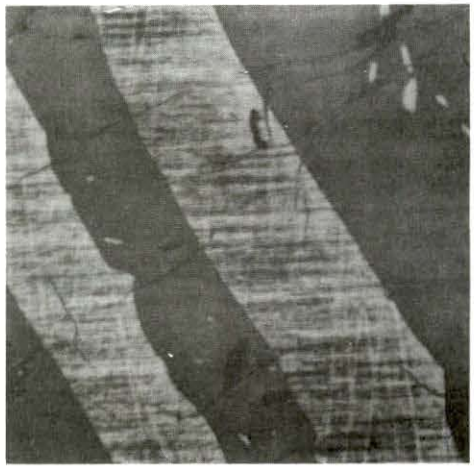

Figure 9. 46.12 a/o Pb, furnace quenched from 1180°C, air etched, streaked area --- $Gd_{11}Pb_{10}$, dark area --- Gd_5Pb_4, light area within dark areas --- Gd_5Pb_3, X200.

Figure 10. 47.64 a/o Pb (essentially pure $Gd_{11}Pb_{10}$), furnace quenched from 1100°C, air etched, X100.

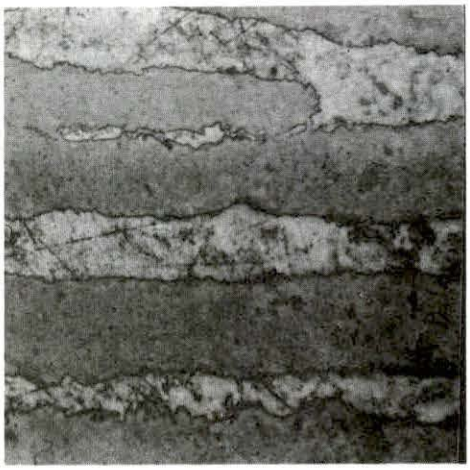

Figure 11. 49.88 a/o Pb, furnace quenched from 1100°C, air etched, dark area --- $Gd_{10}Pb_{11}$, light area --- $\sim Gd_6Pb_7$, X100.

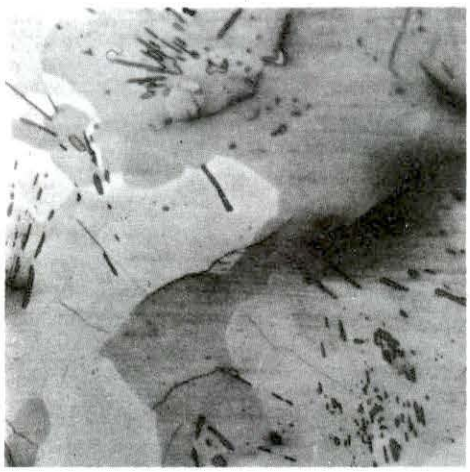

Figure 12. 53.45 a/o Pb furnace cooled, air etched, probably $GdPb_2$ precipitate in $\sim Gd_6Pb_7$ matrix, X250.

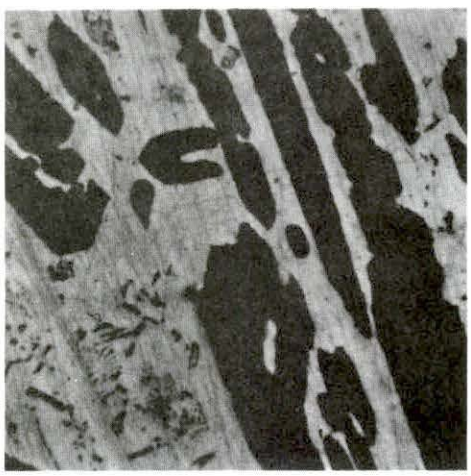

Figure 13. 60.09 a/o Pb, furnace quenched from 900°C, air etched, light area --- $\sim Gd_6Pb_7$ dark area --- $GdPb_2$, X100.

Figure 14. 66.99 a/o Pb, DTA sample, furnace cooled, etched with concentrated H_2SO_4, $GdPb_3$ precipitate in $GdPb_2$, matrix, X500.

Figure 15. 71.29 a/o Pb, furnace cooled, air etched, dark area --- $GdPb_2$, light area --- $GdPb_3$, X50.

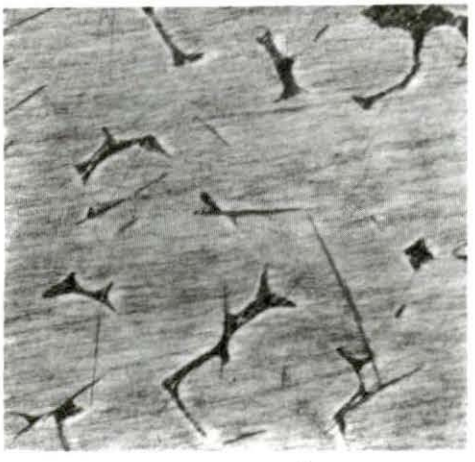

Figure 16. 75.24 a/o Pb, furnace cooled, air etched, X200.

Figure 17. 78.59 a/o Pb, furnace cooled, air etched, light area --- $GdPb_3$, X50.

quenched from approximately 905°C and 1100°C show that Gd_5Pb_3 exists over a solid solution region containing excess lead which precipitates out as Gd_5Pb_4 when cooled. Fig. 7 shows a typical microstructure for alloys between 37.5 and 44 a/o Pb. Figures 8 - 17 show microstructures of alloys between 44 and 78 a/o Pb. The series of photomicrographs agrees well with the phase diagram Fig. 1.

The relative duration of the thermal arrests for each of the compounds was determined from the magnitude of the differential signal at each of the arrest temperatures in the thermal analysis graphs. Gd_5Pb_3 and $GdPb_2$ had the largest thermal arrests while those for Gd_5Pb_4, $Gd_{11}Pb_{10}$ and $GdPb_3$ were all about one third or less the size of the first mentioned compounds. The compound at approximately 54 a/o Pb, designated Gd_6Pb_7, has a very small thermal arrest compared to Gd_5Pb_3 and about one half or less than that of Gd_5Pb_4.

Gd_5Pb_3 melts congruently at 1670 ±5°C and crystallizes in the hexagonal Mn_5Si_3 ($\underline{D}8_8$) type structure, $\underline{a}_o$ = 9.078 ±.004Å and $\underline{c}_o$ = 6.644 ±.005Å. These results agree well with structure and parameters previously reported by Jeitschko and Parthé (6) and by Palenzona and Fornasini (7). The generated and observed $\sin^2\theta$ and intensity data are in complete agreement (see Appendix II).

The Gd_5Pb_4 compound forms by a peritectic reaction at 1460° ±7°C. There is a polymorphic transformation at 1410°C ±7°C. The powder patterns for the α phase (Cu and Fe radiation) were indexed on the basis of the orthorhombic Sm_5Ge_4 type structure having space group Pnma-D_{2h} (8). The best agreement between observed and calculated $\sin^2\theta$ and intensity data (Appendix III) was obtained for a pseudo-tetragonal cell

with $\underline{a} = \underline{c} = 8.20 \pm 0.01$Å and $\underline{b} = 15.62 \pm 0.02$Å.

$Gd_{11}Pb_{10}$, Gd_6Pb_7 and $GdPb_2$ all melt peritectically at 1212 ±7°C, 1155 ±7°C, and 1010 ±2°C respectively. Powder patterns for alloys on and either side of each composition were taken but could not be indexed. Diffractometer traces for polished and etched sections of alloys were also taken but revealed no particular evidence which would help solve the structures.

$GdPb_3$, which melts at 969 ±2°C has the cubic $Cu_3Au(\underline{L1}_2)$ type structure with $\underline{a}_o = 4.8261 \pm .0007$Å. The structure and parameter of the compound have been reported previously by Iandelli (9) and Kuzma et. al. (10) and the value obtained in this investigations agree quite well with Iandelli's value and reasonably well with the Russian results.

DISCUSSION

Through the years, metallurgists, physicists and chemists have searched for laws or rules which will tell them how two or more metals will combine. Most of the rules will work some of the time on some metals. As yet there are no rules which will cover all of the metals in all possible situations. Thus, as more phase diagrams are studied, more information will be available to test the rules that have been proposed.

Gschneidner and Waber (11) have studied the relations that had been proposed and that seem to work well for many metals. They applied them to the known rare-earth binary phase diagrams to see how valid they would be for these alloys. At the time they wrote their paper of all of the possible rare-earth-lead phase diagrams only the lanthanum-lead phase diagram was thought to be reasonably well established. Thus it is interesting to see how well the rules which they have said applied to the rare-earths will apply in the case of the gadolinium-lead binary phase diagram. First let us predict the results and then compare these with the experimental results. The aspects that they considered are size factor, electronegativity, valence, electron numbers and some thermodynamic relationships.

If the sizes of lead (R = 1.750Å) and gadolinium (R = 1.802Å) (12) are considered solid solutions of both lead in gadolinium and gadolinium in lead would be expected since the size difference, 2.8%, is much less than the 15% Hume-Rothery size rule (13). However, size effects should be considered along with electronegativity. The difference in

electronegativity (en_{Pb} = 1.80, en_{Gd} = 1.20) (12) is 0.6 units. If we look at the position of the two metals on a Darken-Gurry plot (14) of electronegativity vs. radius (Fig. 18) it can be seen that lead does not fit inside the ellipse defined by a center at gadolinium, the major axis of ±0.4 electronegativity unit and the minor axis of ±15% variation in radius. If the ellipse were shifted to a center at lead, gadolinium would not fall within this ellipse. Thus, a very limited amount of solid solubility would be expected at either end of the diagram. Complete solid solubility would not be expected because the crystal structures of gadolinium (hcp) and lead (fcc) are different. The maximum solubility of lead in gadolinium is ~ 2 a/o. The lead-rich end of the diagram showed no particular solubility for gadolinium as mentioned previously.

Many times valence compounds, so named for compounds whose ratios are small whole numbers equal to or multiples of the valences of the atoms, are formed. A valence of 3 is commonly assigned to gadolinium and Pauling's valence scheme (15), also uses this value. Lead has been assigned a valence of four by its position in the periodic table but Pauling assigns it a valence of 2.56, and Hume-Rothery and Raynor (13) have considered lead to be divalent. If the common valences associated with gadolinium and lead are used then we would have expected Gd_4Pb_3 to form. This compound does not form but if we use Pauling's scheme we would have to have a compound of $Gd_{2.56}Pb_3$. By coincidence this corresponds approximately to the compound Gd_6Pb_7. This compound is probably not a simple valence compound because there is no corresponding compound in the dysprosium-lead phase diagram (16). By using the Hume-Rothery, Raynor valence a compound of the

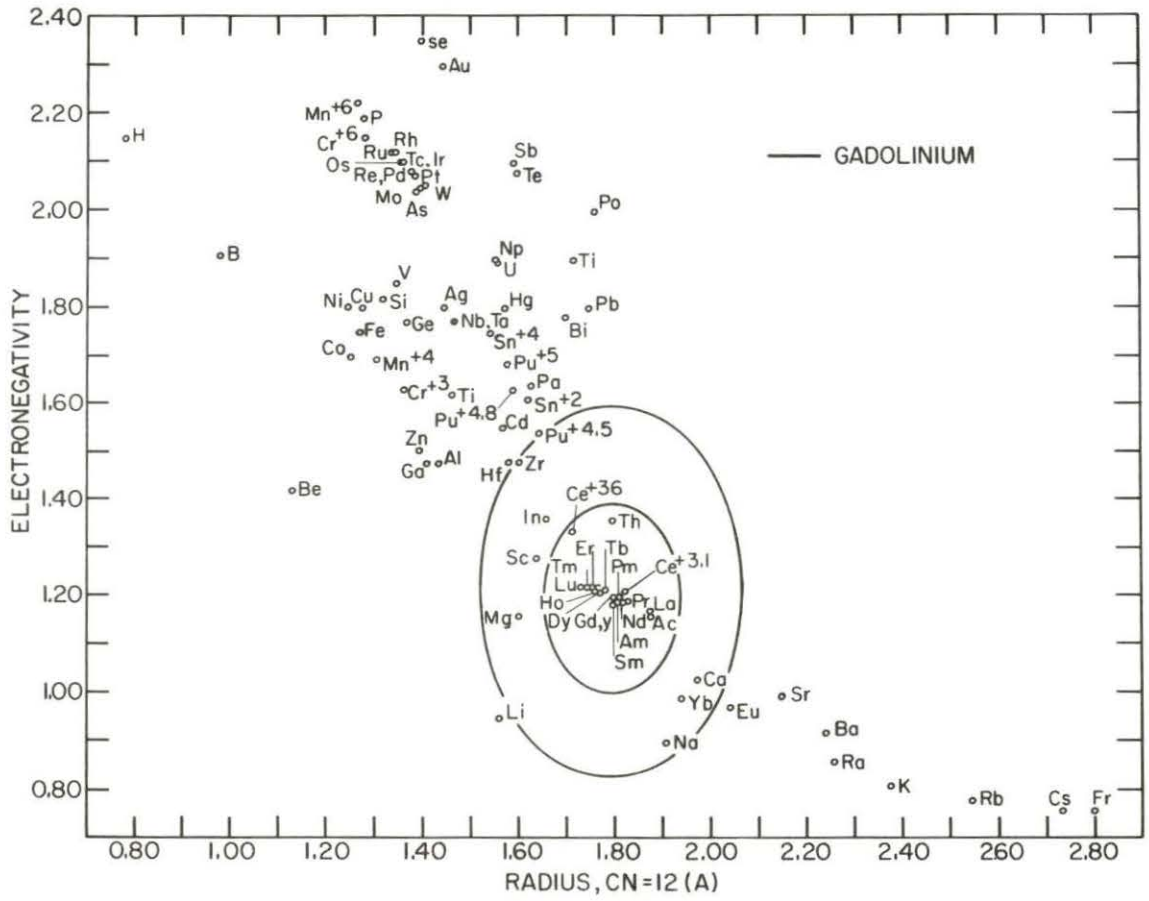

Figure 18. Darken and Gurry plot for gadolinium. Electronegativity vs. radius.

Gd_2Pb_3 stoichiometry is expected but not observed.

The next factors to be considered are the Hildebrand factor (17, 18) and the Mott number (19). Hildebrand originally proposed a quantity defined by H. F. = $1/2\ (V_1 + V_2)\ (\delta_1 - \delta_2)^2$ where V_i is the atomic volume and δ_i is the solubility parameter (equal to $[\Delta H_{subl}/V]^{1/2}$) of the ith atom. If the Hildebrand factor (H. F.) is less than 2RT, that is, when the heat of mixing is less than the thermal energy, then separation of the liquid phases is expected. An H. F. value less than 2RT is obtained for T equal to the melting point of gadolinium and liquid immiscibility for the two metals is incorrectly predicted. If, however, the melting point of lead is used then 2RT is less than the H. F. value and liquid miscibility is correctly predicted.

Mott (19) modified the Hildebrand approach by pointing out that if there is a pronounced tendency of the components to form bonds in solution, the energy of mixing is reduced, and immiscibility is less likely to occur if a number of "bonds" are formed. He defined a bonding number, K, as

$$K = \frac{1/2\ (V_1 + V_2)\ (\delta_1 - \delta_2)^2 - 2RT}{23,060\ (en_1 - en_2)^2}$$

The denominator is the energy in calories of forming a bond between components 1 and 2, if their electronegativities (en_i) are expressed in electron volts. Mott found that if K is less than 2, the metals are generally miscible in all proportions, but if K is larger than 6, immiscibility was to be expected. For values of K from 2 to 6 the size factor of the two constituents would determine whether there would be liquid miscibility.

The Mott bonding number, K, as computed by Teatum, Gschneidner, and Waber (12) for the gadolinium-lead phase diagram is 0.277 at room temperature. At T = 1700°C or ~2000°K the Mott number is less than zero and thus the metals should be miscible throughout the entire temperature range of the investigation. The results show that Mott's bonding number correctly predicts complete miscibility.

Pauling wrote a paper about electron transfer in metal compounds (20) to explain the formation or absence of compounds between two metals. He divided elements into four classes: stable, hypoelectronic (more bond orbitals than electrons), hyperelectronic (less orbitals than electrons) and buffer (can accept or lose electrons without changing valence). Gschneidner and Waber observed that hypoelectronic atoms do not form compounds with the rare earth elements; the hyperelectronic and stable atoms form compounds, while buffer atoms show a gradual transition from non-compound formers to compound formers.

Gschneidner and Waber assigned an electron number to each of the elements on the basis of its position in the periodic chart (see Fig. 19) so that they could put these ideas for compound formation on a somewhat quantitative basis. They found that if the sum of the electron numbers for two elements they were considering was eleven or greater then compounds would be formed in the alloy system. If the sum was nine or less then compounds would not form and those whose sum is in between nine and eleven might or might not form compounds. The rare-earth metals (see Fig. 19) except for europium and ytterbium, are assigned an electron number of three and lead is assigned an electron number of fourteen. Thus their sum is 17 and compound formation would be expected.

PERIODIC CHART OF THE ELEMENTS

Electron No.	1	2	3	4	5	6	7	8	9	10	11	12	13	14	15	16	17	18
																	H	He
	Li											Be	B	C	N	O	F	Ne
	Na											Mg	Al	Si	P	S	Cl	Ar
	K	Ca	Sc	Ti	V	Cr	Mn	Fe	Co	Ni	Cu	Zn	Ga	Ge	As	Se	Br	Kr
	Rb	Sr	Y	Zr	Nb	Mo	Tc	Ru	Rh	Pd	Ag	Cd	In	Sn	Sb	Te	I	Xe
	Cs	Ba	La	Hf	Ta	W	Re	Os	Ir	Pt	Au	Hg	Tl	Pb	Bi	Po	At	Rn
	Fr	Ra	Ac															
	Lanthanides Electron No. =3				Ce	Pr	Nd	Pm	Sm	Eu	Gd	Tb	Dy	Ho	Er	Tm	Yb	Lu
	Actinides				Th	Pa	U	Np	Pu	Am	Cm	Bk	Cf					
Electron No.					4	5	6	6	5	4	3(?)	3(?)	3(?)					

Figure 19. Electron numbers assigned for each element on the basis of their position in the periodic table.

The logical extension pointed out by Gschneidner and Waber is that the number of compounds ought to depend in some way on the electron number. A graph of the number of compounds vs. the summation of electron numbers of the known systems at the time Gschneidner and Waber wrote their discussion is shown in Fig. 20. An estimate of three to four compounds for the gadolinium-lead system is made from the data in Fig. 20. Experimentally six intermetallic compounds were found in this system. The prediction does demonstrate the correct trend even if it does not give the correct number.

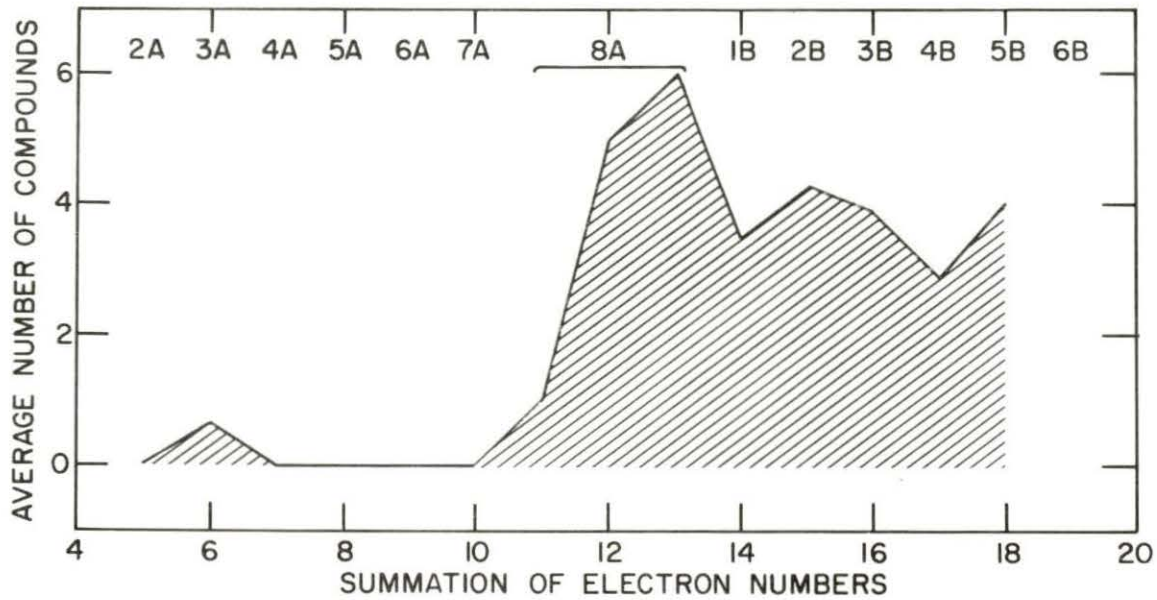

Figure 20. Average number of compounds vs. the summation of electron numbers.

SUMMARY

If a prediction were to have been made for the gadolinium-lead phase system from presently known and accepted rules and empirical relations the following would have been expected: very little terminal solid solubility, complete miscibility and three or four intermetallic compounds. These predictions are correct as far as they go except for the number of compounds predicted. The actual data shows that the addition of lead lowers the α-β transformation of gadolinium from 1258°C to 1212°C, and the gadolinium melting point 1313°C to a eutectic reaction at 14.5 a/o Pb and 1120°C. The addition of gadolinium raises the melting temperature of lead from 327°C to 328°C. The room temperature solid solubility for both metals is negligible. Of the six compounds formed one, Gd_5Pb_3 melts congruently at 1670°C and the rest, Gd_5Pb_4, $Gd_{11}Pb_{10}$, Gd_6Pb_7, $GdPb_2$ and $GdPb_3$, form peritectically at 1460°C, 1225°C, 1160°C, 1010°C and 969°C, respectively. In addition there is a polymorphic transformation in Gd_5Pb_4 at 1140°C. The crystal structures for Gd_5Pb_3 and $GdPb_3$ were reported previously to have the Mn_5Si_3 ($\underline{D}8_8$) and $AuCu_3$ ($\underline{L}1_1$) structures, respectively, and these results were confirmed in this investigation. The α phase of Gd_5Pb_4 was indexed on the basis of a pseudo-tetragonal modification of the Sm_5Ge_4 orthorhombic structure (Pmna) with $\underline{a} = \underline{c}$. Although the other compounds were investigated, their crystal structures were not solved.

From the practical aspect, it was found that most of the Gd-Pb alloys which would be useful for higher temperature reactor applications

were very reactive with air and quite brittle. Therefore they would have to be alloyed with some other element to reduce oxidation or clad with another substance to provide a useful, workable alloy.

BIBLIOGRAPHY

1. Handbook of Nuclear Technology, McGraw-Hill Book Co., Inc., New York, New York, ca. 1959.

2. F. H. Spedding and A. H. Daane, U. S. Atomic Energy Comm. Rept. ISC-902, 1957, p. 19.

3. W. Jeitschko and E. Parthé: A Fortran IV Program for the Intensity Calculation of Powder Patterns, Univ. of Pennsylvania, Laboratory for Research on the Structure of Matter, ca. 1965.

4. R. E. Vogel and C. P. Kempter, U. S. Atomic Energy Comm. Rept. LA-2317, 1959.

5. D. H. Dennison, M. J. Tschetter and K. A. Gschneidner, Jr., J. Less-Common Metals, 1966, vol. 10, p. 108.

6. W. Jeitschko and E. Parthé: Acta Cryst., 1967, vol. 22, p. 551.

7. A. Palenzona and M. L. Fornasini: Atti Accad. Naz. Lincei Rc., 1966, vol. 40, p. 1040.

8. G. S. Smith, Q. Johnson and A. G. Tharp: Acta Cryst., 1967, vol. 22, p. 269.

9. A. Iandelli: Atti Accad. Naz. Lincei Rc., 1960, vol. 29, p. 62.

10. Yu. B. Kuzma, R. V. Skolozdra and V. Ya. Markiv: Dopovidi Akad. Nauk Ukr. RSR, 1964, vol. 8, p. 1070.

11. K. A. Gschneidner, Jr. and J. T. Waber: p. 386 in The Rare Earths, F. H. Spedding and A. H. Daane, eds., John Wiley and Sons, New York, New York, and London, England, 1961.

12. E. Teatum, K. A. Gschneidner, Jr. and J. T. Waber: U.S. Atomic Energy Comm. Rept. LA-2345, 1960.

13. W. Hume-Rothery and G. V. Raynor: Structure of Metals and Alloys, 3rd ed., Inst. of Metals, London, England, 1954.

14. L. S. Darken and R. W. Gurry: Physical Chemistry of Metals, McGraw-Hill Book Co., Inc., New York, New York, 1953.

15. L. Pauling: Theory of Alloy Phases, Amer. Soc. Metals, Cleveland, Ohio, 1955.

16. O. D. McMasters, T. J. O'Keefe and K. A. Gschneidner, Jr.: Dysprosium-Lead System, to be published Trans. Met. Soc. AIME, 1968.

17. J. H. Hildebrand: J. Am. Chem. Soc., 1926, vol. 51, p. 66.

18. J. H. Hildebrand and R. L. Scott: The Solubility of Nonelectrolytes, 3rd ed., Reinhold Publishing Corp., New York, New York, 1950.

19. B. W. Mott: Phil. Mag., 1957, ser. 8, vol. 2, p. 259.

20. L. Pauling: Proc. Natl. Acad. Sci., 1950, vol. 36, p. 533.

ACKNOWLEDGEMENTS

The author wishes to thank his associates in Metallurgy Group IX, especially O. D. McMasters for his help with the x-ray work. Thanks are also due to B. Beaudry for his help in the thermal analysis and to H. Baker for some of the metallographic work.

APPENDIX I

APPENDIX I

The Impurities in the Gadolinium and Lead Used in This Investigation[1]

Element	Gadolinium				Lead	
	Sample 1 ppm	Sample 2 ppm	Sample 3 ppm	Sample 4 ppm	Comnico Analysis ppm	Spectroscopic group analysis ppm
H	18	18	23	10		
C	102	90	100	45		
N	60	16	30	1		
O	411	170	630	521		
F	81	1	17	11		
Na		20	10			
Mg		2		1	0.1	vft[2]
Al		10	20	10	nd[3]	
Si	3		10	50	0.1	ft[4]
Cl		20				
K		70				
Ca	425	30	50	30	0.1	ft
Sc	0.6	5.7				

[1] Impurities listed are maximum amounts

[2] Very faint trace

[3] Not detected

[4] Faint trace

APPENDIX I (continued)

Element	Gadolinium				Lead	
	Sample 1 ppm	Sample 2 ppm	Sample 3 ppm	Sample 4 ppm	Comnico Analysis ppm	Spectroscopic group analysis ppm
V					nd	
Cr	10	10	10		nd	
Mn		40			nd	
Fe	31	0.7	30	30	0.1	t[5]
Ni		1	10	100	nd	
Cu		20	10	5	0.2	ft
Zn		3			nd	nd
As						nd
Y	20	4	0.6	20		
Mo		3				
Ag		3			0.1	nd
Cd					nd	t
In					nd	
Sn		20			nd	
Sb						nd
La		50				
Ce	6	1.4				
Pr	6	8.7				
Nd	1	4	500			
Sm	200	4	1	200		
Eu	10	100	1	100		

[5] Trace

APPENDIX I (continued)

	Gadolinium				Lead	
Element	Sample 1 ppm	Sample 2 ppm	Sample 3 ppm	Sample 4 ppm	Comnico Analysis ppm	Spectroscopic group analysis ppm
Tb	100	500	3	500		
Dy			8	100		
Ho		2	2.7	500		
Er		1	0.4			
Tm		2	0.3			
Yb		9	5			
Lu			6.6			
Hf		5				
Ta	200	12	500	300		
W		8				
Re		2				
Os		3				
Ir		2				
Pt		4				
Au		2				
Tl					nd	nd
Pb		30				
Bi					1.0	ft

APPENDIX II

Intensity Calculation for Gd_5Pb_3 with Mn_5Si_3 ($\underline{D8}_8$) Structure Type.
Copper Radiation; $\underline{a}_o = 9.078 \pm .004$Å, $\underline{c}_o = 6.644 \pm .005$Å.

I_o	$\sin^2\theta_o$	h k l	$\sin^2\theta_c$	I_c
W	.0427	1 1 1	.0423	46.4
M	.0545	0 0 2	.0539	226.9
VW	.0668	1 0 2	.0635	75.5
M	.0683	2 1 0	.0673	260.6
VS	.0815	2 1 1	.0808	1000.0
S	.0834	1 1 2	.0827	650.4
S	.0872	3 0 0	.0865	282.2
W	.0931	2 0 2	.0923	151.9
W	.1261	3 1 0	.1250	68.1
W	.1294	2 2 1	.1288	72.4
M	.1389	3 1 1	.1385	212.0
VW	.1510	1 1 3	.1500	8.9
		4 0 0	.1538	12.8
M	.1698	2 2 2	.1692	94.5
S	.1892	2 1 3	.1885	287.8
W	.1963	3 2 1	.1961	42.6
W	.2024	4 1 0	.2019	60.4
W	.2084	4 0 2	.2077	43.5
M	.2163	0 0 4	.2154	102.0
MW	.2363	3 2 2	.2365	63.4
MW	.2472	3 1 3	.2461	86.9
VW	.2691	4 2 0	.2692	67.5
W	.2726	3 3 1	.2731	105.6
W	.2829	4 2 1	.2827	41.5
		2 1 4	.2827	60.3
M	.2944	5 0 2	.2942	202.3
W	.3024	3 0 4	.3019	83.3
W	.3124	3 3 2	.3134	69.6
VVW	.3228	4 2 2	.3231	19.4
VVW	.3408	3 1 4	.3404	28.3
VVW	.3682	4 3 1	.3692	21.4
VVW	.3809	3 3 3	.3808	62.0
VVW	.3895	4 2 3	.3904	25.0
VVW	.3993	6 0 2	.3999	43.9
VW	.4046	2 1 5	.4039	85.0
VVW	.4123	6 1 0	.4134	40.8
VVW	.4164	4 1 4	.4173	37.4
VVW	.4549	5 0 4	.4558	51.0
VW	.4840	4 2 4	.4846	55.7
VVW	.4936	1 0 6	.4942	3.4
VW	.5120	6 2 1	.5134	42.8

APPENDIX II. (continued)

I_o	$\sin^2\theta_o$	h k l	$\sin^2\theta_c$	I_c
W	.5240	7 0 2 5 3 2	.5250	77.9
VW	.5607	7 1 1	.5615	21.5
VW	.6177	6 3 1	.6192	65.2
VW	.2670	6 1 4	.6288	55.1
W	.6580	6 3 2	.6596	63.2
W	.6671	8 0 2	.6692	42.9
W	.7256	5 0 6	.7250	83.6

APPENDIX III

Intensity Calculation for Gd_5Pb_4 with Sm_5Ge_4 Structure Type. (Pnma-D_{2h}^{16})
Copper Radiation; $\underline{a} = \underline{c} = 8.20 \pm .01$Å, $\underline{b} = 15.62 \pm .02$Å.

I_o	$\sin^2\theta_o$	h k l	$\sin^2\theta_c$	I_c
VW	.0276	1 2 1	.0274	30.7
MW	.0393	1 3 1	.0396	216.4
W	.0462	1 1 2 (211)[1]	.0466	3.8
MW	.0541	2 2 1 (122)	.0539	211.9
VS	.0668	2 3 1 (132)	.0661	1429.8
M	.0704	2 0 2	.0707	421.5
MS broad	.0737	2 1 2	.0731	85.5
		2 4 0 (042)	.0743	678.1
M	.0789	1 5 1	.0786	262.3
W	.0795	2 2 2	.0804	98.3
W	.0805			
W	.0816	0 1 3	.0820	28.2
S	.0832	2 4 1 (142)	.0832	680.1
M	.0882	0 6 0	.0877	347.6
		1 0 3 (301)	.0844	348.6
S	.0902	3 1 1 (113)	.0902	836.3
		2 3 2	.0926	1.9
MW	.0955	2 5 0	.0962	94.1
		3 2 1 (123)	.0981	5.6
MW	.1043	2 5 1 (152)	.1050	132.7
W	.1101	3 3 1 (133)	.1103	45.8
W	.1143	2 0 3 (302)	.1149	166.8
W	.1236	2 6 0 (062)	.1230	1.0
		0 7 1	.1282	5.5
VW	.1293	2 5 2	.1316	29.7
		2 6 1 (162)	.1319	9.0
MS	.1377	2 3 3 (332)	.1368	81.5
		1 7 1	.1370	226.5
VW	.1413	4 0 0 (004)	.1414	12.9
VW	.1451	4 1 0	.1438	21.7
MS	.1493	1 5 3 (351)	.1493	418.8
W	.1521	1 1 4 (411)	.1527	124.9
W	.1551	2 7 0	.1547	19.0
		0 8 0	.1559	75.1
		2 6 2	.1584	56.7
M	.1580	3 0 3	.1591	36.8
		4 2 1 (124)	.1599	60.8

[1] Due to the pseudotetragonal structure there are two planes which have the same $\sin^2\theta$ value.

APPENDIX III. (continued)

I_o	$\sin^2\theta_o$	h k l	$\sin^2\theta_c$	I_c
		1 1 3	.1615	8.1
VW	.1623	4 3 0	.1633	26.1
		1 7 2 (271)	.1634	10.5
W	.1686	3 2 3	.1688	5.6
M	.1734	4 3 1	.1722	136.8
		1 8 1	.1736	0.2
MW	.1767	3 6 1	.1761	104.7
		4 0 2	.1768	84.8
VW	.1794	2 1 4	.1792	52.7
W	.1822	4 4 0	.1804	9.5
		3 3 3	.1810	11.8
W	.1847	4 2 2	.1865	18.0
W	.1844	4 4 1	.1892	7.1
VW	.1968	3 4 3	.1981	83.8
		4 3 2	.1986	22.5
VW	.2005	2 8 1	.2001	13.9
VW	.2070	0 9 1	.2061	13.4
		3 7 1	.2077	39.0
VW	.2165	3 5 3	.2200	72.0
		3 0 4	.2210	14.6
VW	.2237	3 1 4	.2234	10.0
		0 1 5		
VW	.2340	2 7 3	.2342	91.0
VW	.2399	1 9 2	.2415	57.3
VW	.2518	5 3 1	.2517	23.9
		3 4 4	.2599	18.1
M	.2617	4 7 0	.2608	57.1
		1 1,0 1	.2613	2.9
M	.2666	5 2 2	.2661	72.7
M	.2697	4 7 1	.2696	156.1
M	.2776	3 7 3	.2784	84.4
		0, 10, 2	.1789	168.0
		0 5 5	.2818	43.1
M	.2836	4 0 4	.2828	45.
		4 1 4	.2853	72
		1 9 3	.2857	126.3
W	.2870	1, 10, 2	.2878	81.1
M	.2909	5 5 1	.2907	103.6
M	.2958	5 4 2	.2953	107.2